Cement and Concrete Research 173 (2023) 107298

Contents lists available at ScienceDirect

Cement and Concrete Research

journal homepage: www.elsevier.com/locate/cemconres

Development of durable engineered cementitious composites using local ingredients

He Zhu [a], Yichao Wang [b], Mohammed Mehthel [c], Thibault Villette [c], Oscar Salazar Vidal [c], Waleed N. Nasser [c], Victor C. Li [a,*]

[a] Department of Civil and Environmental Engineering, University of Michigan, Ann Arbor, MI 48109, USA
[b] School of Civil Engineering, Shijiazhuang Tiedao University, Shijiazhuang, Hebei Province 050043, China
[c] Saudi Aramco, Dhahran 31311, Saudi Arabia

ARTICLE INFO

Keywords:
Engineered cementitious composites (ECC)
Desert sand
Crystalline admixture
Self-healing
Crack control
Permeability

ABSTRACT

Environmental and economic concerns impel large volume construction materials to employ as many local ingredients as feasible while maintaining high performance. In this research, durable Engineered Cementitious Composites (ECC) are developed using local desert sand from Saudi Arabia, polypropylene/polyethylene fibers, and crystalline admixture. Multi-scale characterization methods were utilized, including compressive/uniaxial tensile tests, self-healing tests, permeability tests, and micro/chemical analyses. Mercury intrusion porosimetry, X-ray diffraction, and scanning electron microscopy were employed to interpret the mechanisms underlying the observed macroscopic behavior. The developed ECC possesses the highest ductility (8.6 %) and lowest crack width (below 63 μm) among desert sand ECCs in the literature. The crystalline admixture produces additional C-S-H gel and crystalline $Ca(OH)_2$ precipitates, endowing the desert sand ECC with enhanced self-healing ability. The self-healed ECC demonstrates improved durability with reduced permeability and enhanced mechanical properties recovery. The localized durable ECC holds promise for both rehabilitating aging infrastructures and newly constructed facilities in regions with large supplies of desert sand.

1. Introduction

Newly constructed facilities and aging infrastructure repair demand a large volume of concrete, which accounts for over 80 % of total engineered material consumption by weight globally [1]. As concrete's essential ingredient, cement production is responsible for 5–8 % of global CO_2 emissions. Portland cement ranks as the third-largest source of anthropogenic emissions following power plants and steel production [2]. Construction is inherently local. Sustainable practice and economic considerations dictate the use of as many local materials as feasible.

Poor field durability limits the sustainability of concrete infrastructure [3,4]. Due to its very low tensile strength, conventional concrete is susceptible to cracking caused by imposed deformations and loads [5,6]. Cracks jeopardize structural durability, especially when exposed to water environments, such as pipes, dams, and channels [7]. Water and corrosive ions penetrate cracks, causing further deterioration of the concrete structure. The brittle nature of concrete results in the requirement of repeated maintenance, enlarging the carbon and energy footprints of civil infrastructure and impairing the sustainability of the built environment.

Engineered cementitious composites (ECC) is a fiber reinforced concrete designed for high tensile ductility (>3 %) and tiny crack width (usually below 100 μm at failure) [4]. Ductile ECC suppresses brittle fracture and converts the macro crack into many micro-cracks. Moreover, ECC has the ability of autogenous healing due to the intrinsically small crack width, significantly reducing the permeability of ECC materials [8–10] in structures. To attain the strain-hardening effect, coarse aggregate is eliminated from ECC as required by micromechanics theory [4]. The absence of coarse aggregate leads to a high cement volume in conventional ECC compositions, contributing to a high embodied carbon footprint [11]. In addition, the use of fiber reinforcement significantly increased the material cost by 1–3 times depending on the fiber types [10]. Although ECC has been successfully demonstrated in repairing or constructing infrastructures due to its high-performance (high ductility, controlled crack width, and inherent self-healing), continued efforts are necessary to drive down the embodied CO_2 and material cost.

* Corresponding author.
E-mail addresses: zhuhe14@tsinghua.org.cn (H. Zhu), wangyichao@stdu.edu.cn (Y. Wang), mohammed.mehthel@aramco.com (M. Mehthel), thibault.villette@aramcouk.com (T. Villette), oscardaniel.salazarvidal@aramco.com (O.S. Vidal), waleed.nasser@aramco.com (W.N. Nasser), vcli@umich.edu (V.C. Li).

https://doi.org/10.1016/j.cemconres.2023.107298
Received 31 October 2022; Received in revised form 1 August 2023; Accepted 3 August 2023
Available online 8 August 2023

Sustainable ECC can be developed strategically by utilizing low-cost and low-carbon ingredients. ECC compositions typically include cementitious material, fine silica sand, and fibers. While cement amounts to over 75 % of the embodied carbon in a classic M45 mixture [4,10], supplementary cementitious materials (SCM), such as fly ash (FA) [12], limestone [10], calcined clay [11], rice husk ash [13], recycled fine powder [14], and iron ore tailings [15], have been adopted to replace portland cement in ECC. Among various SCMs, FA has proven to be one of the best substitutions of OPC in ECC due to its wide availability, as well as superior tensile ductility and tight crack width of FA-based ECC [4,16,17]. However, high volume of FA can compromise tensile strength and may also limit the self-healing ability. Hence, the substituted ratio of FA to cement should be carefully designed to obtain the desired material greenness, mechanical performance, and self-healing capacity.

Besides binders, F75-manufactured silica sands (average diameter of 110 μm) are typically adopted as fine aggregates, which increases the ECC cost. Especially when manufactured sand is unavailable for local regions, long-distance transportation further aggravates the cost concern and CO_2 emission. Natural sand (e.g., river sand, sea sand, and gravel sand) have been investigated for developing ECC [18–20]. ECCs with gravel sand or crushed sand with a maximum diameter of up to 2.4 mm have attained a comparable tensile strain capacity to silica sand ECC (2–3 %) [20]. River sand ECC can reduce by 10 % material cost, however, the crack width under load is larger than 100 μm [18,21], limiting the self-healing ability. Moreover, scarcity, rising prices, and environmental concerns due to excessive dredging limit the exploitation of river sand. While sea sand ECC (up to 4.75 mm) has been developed [19], its application is limited to structures with non-corrosive reinforcement and in offshore regions [22].

Owing to its low cost and abundant availability, desert sand has attracted increasing attention for concrete applications [23–27]. Strength reduction has been observed in desert sand concrete compared to normal sand concrete. Factors such as poor gradation [23], round shape [25], salt ions [26], and entrained air void [28] have been suggested as reasons for the compromised strength of concrete. Remarkably, these adverse factors of desert sand in concrete may in fact act as advantages when used in ECC composition. For example, the very fine particle size and the round morphology of desert sand decrease the fracture toughness of the matrix, facilitating the initiation of microcracks and enabling their extension in a steady flat crack mode [4,29] favorable for multiple cracking of ECC.

Some explorations of desert sand ECC (DS ECC) have been conducted in regions with large local supplies, including Saudi Arabia [30], Australia [24,31], and China [26,32]. Similar to desert sand concrete, ECC also experiences a strength reduction with the increased replacement ratio of desert sand to silica sand [32,33]. Further, by substituting silica sand with desert sand, the tensile ductility is also depressed to 1–2 % [30,31]. As yet, few studies of DS ECC focus on crack width control, which is a critical factor determining durability (such as the permeability and self-healing performance), suggesting that more studies regarding the matrix design, high ductility, and crack control of desert sand ECC are needed.

To the best knowledge of the authors, the emerging researches of DS ECC all employ polyvinyl alcohol (PVA) fibers as reinforcement [24,26,30–32]. The high cost and limited supply source weaken the competitiveness of PVA fibers in ECC applications [22]. Besides PVA fibers, domestically available polypropylene (PP) [10] and polyethylene fibers (PE) [34] have been used in ECC compositions. PP fibers are low cost as well as low strength compared to PVA fibers, while PE fibers have higher tensile strength and moderate cost, indicating that hybrid PE/PP fibers can be an alternative reinforcement for DS ECC. However, PP ECC [10,35] and PE ECC [34] have been reported with larger crack widths (>100 μm) than PVA ECC (< 70 μm) due to their hydrophobic surface. Crack width is critical for determining the autogenous healing efficiency of ECC. The maximum healable crack width depends on various factors, including the concrete age, healing agents, working environments, etc. Existing findings are contradictory regarding the maximum healable crack width (10–300 μm, or even higher than 1000 μm) [36,37] which may depend on how deep into the crack healing is observed. Crack width below 50 μm is preferred for autogenous robust self-healing of ECC [8,10,38].

Self-healing of cementitious material is realized by further hydration and precipitation of calcium carbonate [39]. Robust self-healing effect can be attained via controlled crack width and enhanced healing product generation [36]. Although some enhanced healing methods such as encapsulated healing agents [40], bacteria [41], and superabsorbent polymers [42] have been explored for self-healed concrete, limitations remain to hinder their applicability. For example, the encapsulated agent requires more preparation work and is prone to break during mixing [40]. To facilitate the healing efficiency of bacteria, many prerequisites should be met, such as the compatibility between bacteria (type, nutrient medium, concentration) and concrete (temperature, PH, and service conditions) [37,41,43–46]. While superabsorbent polymers can release preabsorbed water to suppress early age cracking, their super water absorbent capacity imposes mixing challenges on producing high-performance ECC with a low water/binder ratio.

Due to the compatibility with cementitious material, the crystalline admixture (CA) is used for reducing the permeability and increasing the healing capacity of concrete [39,40,47]. Although proprietary formulations of CA are confidential, CA is generally a synthetic cementitious material containing reactive silica, cement, and some crystalline catalysts [48], some publications also mention carbonates, silicates, aluminates, tetrasodium EDTA, glycine, and sodium acetate [49]. Under the presence of water, the active chemicals react with tricalcium silicates or calcium hydroxide (CH) to form crystalline products which disconnect pores and seal cracks in the concrete [50,51]. With 0.5—3 % binder weight dosage, CA usually has no negative effect on the compressive strength of concrete [49]. Cracks up to 400 μm of cracks can be healed and the healing effect has been validated even after two years [49,52–56].

High-Performance Fiber Reinforced Concrete (HPFRC) has been demonstrated with higher self-healing properties than conventional concrete due to its lower water/binder content and controlled crack width owing to the high fiber content [57]. Especially when combined with slag, nanocellulose, or calcium sulphoaluminate cement (CSA), CA could promote crack closure of HPFRC even up to 500 μm or higher [58]. Moreover, Moreover, the synergetic effect PVA fibers and CA that boosted the $CaCO_3$ precipitation on the fiber's surface have been reported, while this specific mechanism is different for PP or steel fibers [49]. Ferrara et al. found that strength and stiffness could be recovered once the crack closure exceeded 60—80 % [59], and the healing products provided sealing even after repeated loading [60]. However, the ductility of HPFRC decreased after healing [56].

Similarly, an increased closure rate of cracks is observed by adding crystalline admixture in ECC, however, the permeability and mechanical recovery of the cracked ECC remain to be investigated [61]. Moreover, incorporating crystalline admixture in a greener ECC (high fly ash volume, desert sand, and PP/PE fiber) demands comprehensive designs, including crack width control, self-healing efficiency, permeability reduction, and mechanical properties recovery (tensile strength and ductility).

The objective of this study is to develop a durable ECC using local materials (desert sand and PP/PE fibers), which possesses the advantage of availability, low cost, and low carbon footprint (associated with long-distance transport) while maintaining high performance, i.e., ultra-high ductility (>8 %), tiny crack width (around 60 μm at failure), and robust self-healing ability. To do so, a crystalline capillary waterproofing admixture was employed to enhance the healing capacity. Multi-scale characterization methods were utilized to evaluate the performance of DS-ECC at the micro and macro scales. Material properties were experimentally studied by compression, uniaxial tension, self-healing,

Table 1
Chemical compositions of cement and fly ash (%).

Ingredients	CaO	Al_2O_3	SiO_2	Fe_2O_3	MgO	SO_3	K_2O	TiO_2
OPC	63.5	4.8	19.6	2.9	2.2	2.6	0.6	0
CSA	47.2	10.1	7.0	0.7	1.1	33.1	0.1	0
FA	10.8	16.2	51.6	5.0	3.7	1.4	2.5	0
ML300D	57.5	5.0	20.0	2.5	2.7	4.7	1.2	5.7

Table 2
Material properties of crumb rubber (%).

Acetone extract	Ash content	Carbon black	Rubber hydrocarbon
13 ± 7	≤10	32 ± 6	≥42

and permeability tests. Micro/chemical analysis with mercury intrusion porosimetry (MIP), X-ray Diffraction (XRD), and scanning electron microscope-energy dispersive spectroscopy system (SEM-EDS) were conducted to understand the underlying mechanisms of the macroscopic behavior.

2. Experimental program

2.1. Mixture design

Five mixtures were designed for durable desert sand ECC (DS-ECC). 25 % of ordinary Portland cement (OPC) was replaced with calcium sulphoaluminate cement (CSA) to mitigate drying shrinkage [11,62]. The binder system contains cement (OPC + CSA) and fly ash (FA), where the weight ratio of FA/(OPC + CSA) was 2.2. Crumb rubber powders (with an average particle size of 275 μm) work as artificial flaws to induce multiple cracks [63]. Tables 1–2 lists the chemical compositions of OPC, CSA, FA, and crumb rubber (CR). The water to binder ratio was

Table 3
Properties of PE and PP fiber.

Fiber type	Diameter (μm)	Length (mm)	Nominal strength (GPa)	Young's Modulus (GPa)	Rupture elongation (%)	Density (g/cm^3)
PP	12	10	0.85	6	21	0.91
PE	24	12	2.90	100	2.42	0.97

Table 4
Mixture design of ECC using desert sand (kg/m^3).

Mixture	OPC	CSA	FA	Sand	W	ML300D	CR	PE	PP	Bulk density
SS	300	100	880	384	346	0	30	10	9	1902
DS-M0	300	100	880	384	346	0	30	10	9	1890
DS-M2	300	100	880	384	346	26	30	10	9	1895
DS-M2'	300	100	880	384	346	26	60	10	9	1803
DS-M4	300	100	880	384	346	52	30	10	9	1900

Note: The dosage of the water reducer (MasterGlenium 7920 from BASF) was 2 kg/m^3 for all mixtures.

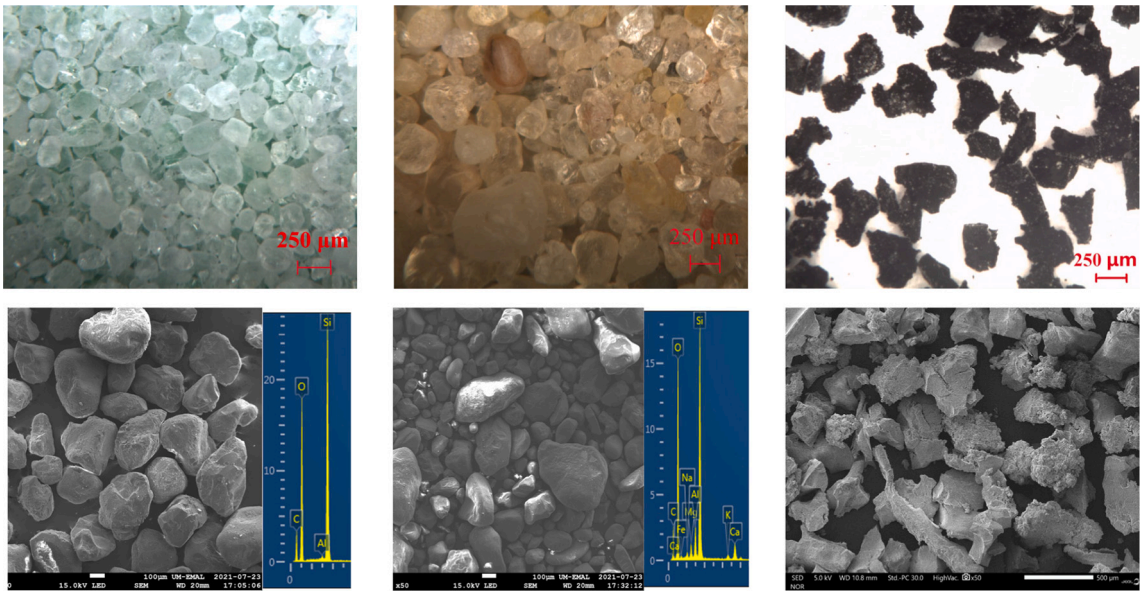

(a) Silica sand (F75) (b) Desert Sand (c) Crumb rubber

Fig. 1. Morphological information of sands and crumb rubber. (Silica sand, Si:O = 42.3:57.3 by EDS; desert sand, Si:O:Ca:Al:Fe:Mg = 30.4:55.7:4.4:3.7:2.1:1.8). (For interpretation of the references to colour in this figure legend, the reader is referred to the web version of this article.)

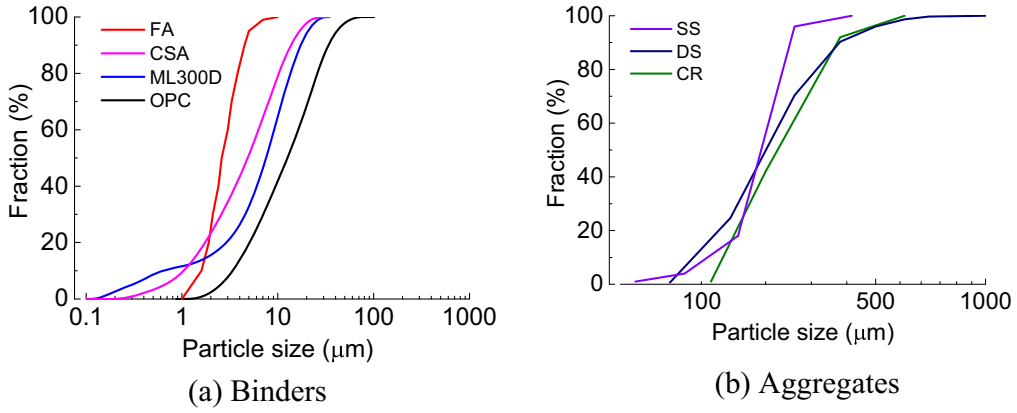

Fig. 2. Particle size distributions of dry ingredients.

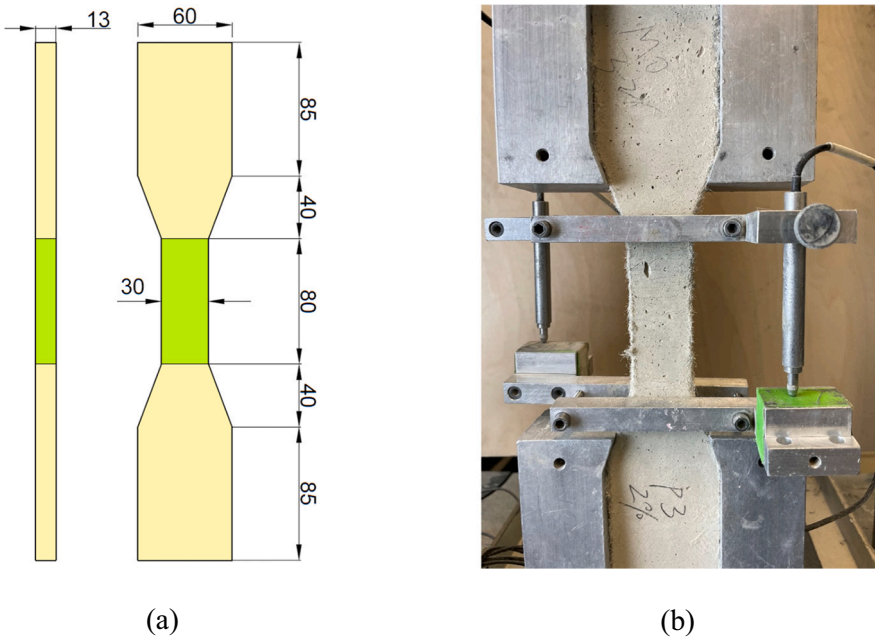

Fig. 3. Dogbone-shaped specimen for uniaxial tension (a) showing dimensions (Unit: mm) and (b) the grip and LVDT set up during loading in a load frame.

maintained as 0.27. Desert sand obtained from Saudi Arabia was utilized with a 0.3 mass ratio of the binder. To obtain the robust strain-hardening effect while reducing the material cost, a hybrid of approximately 1 % polyethylene (PE) and 1 % polypropylene (PP) fibers in volume were used, of which the geometric and mechanical properties are listed in Table 3.

A commercially available crystalline capillary waterproofing admixture from BASF (MasterLife 300D, or ML300D) was employed to facilitate the crack sealing. According to the manufacturer's technical sheet, ML300D mainly consists of cement, sodium carbonate, quartz, and limestone. It produces additional C-S-H gel and crystalline precipitates to fill pores and capillaries, helping initiate and facilitate insoluble crystal growth in the cracks. As suggested by the manufacturer, 0 %/2 %/4 % binder weight of ML 300D was adopted to determine the optimal dosage for enhancing the self-healing ability of DS-ECC, named DS-M0, DS-M2, and DS-M4 in Table 4. These mixes all have 30 g/L of crumb rubber (CR). The mix DS-M2' is included to investigate the effect of higher CR content (60 g/L) on crack width and tensile performance. F75 manufactured silica sand was selected as a benchmark to demonstrate the difference between DS ECC and silica sand ECC (Mixture SS). Fig. 1 shows the images of desert sand and silica sand, and their particle size distributions can be found in Fig. 2.

Table 5
Experimental protocol of the DS-ECC.

Mixture	Compressive strength	Uniaxial tensile test	Self-healing test	Permeability test
SS	√	√	√	X
DS-M0	√	√	√	√
DS-M2	√	√	√	√
DS-M2'	√	√	X	X
DS-M4	√	√	X	X

√ = measured items.
X = not measured items;

2.2. Specimens preparations

The dry ingredients (OPC, CSA, FA, sand, ML300D, CR) were premixed for 10 min using a 5.7 L planetary mixer at 100 rpm. Then water associated with the water reducer was added and further mixed for 5 min at 100 rpm. Finally, fibers (1 % volume of PE and 1 % volume of PP) were added to the fresh materials and mixed at 200 rpm for an

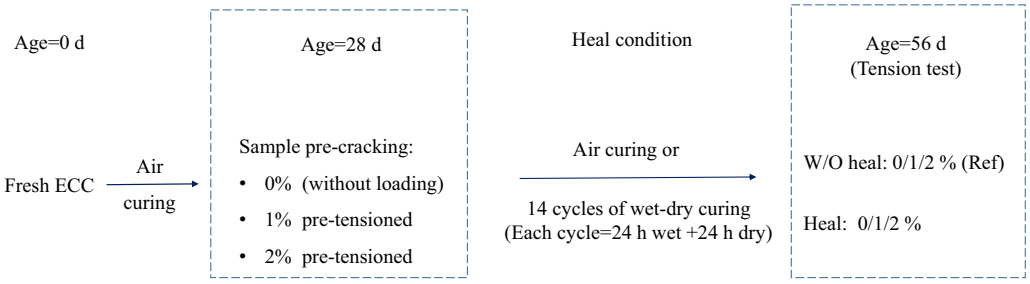

Fig. 4. Experimental process of self-healing test.

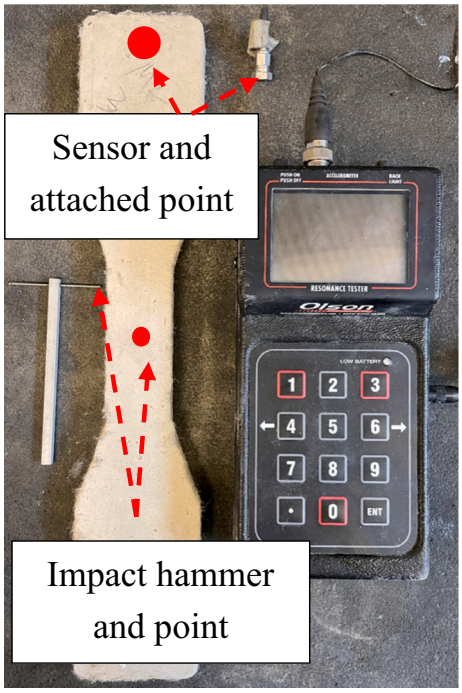

Fig. 5. Resonance frequency test.

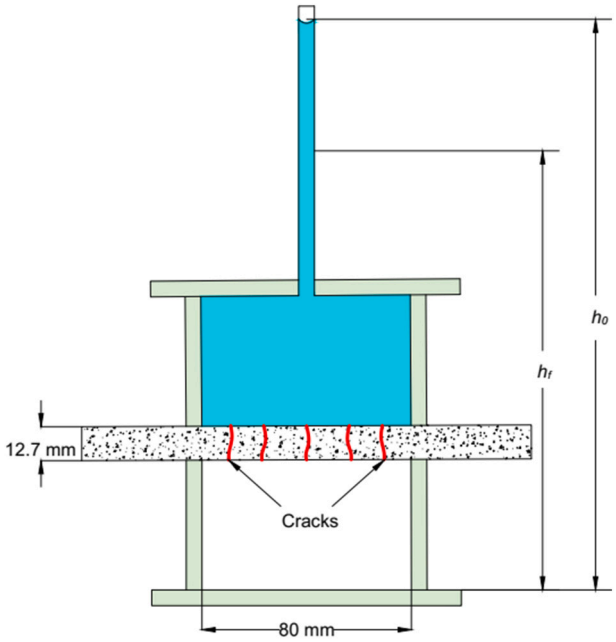

Fig. 6. Permeability test.

additional 5 min. After obtaining a homogeneous fiber dispersion, the fresh ECC was cast into 50 mm-cube and dogbone-shaped molds (Fig. 3). After curing in air (20 ± 3 °C, 40 ± 5 % RH) for 28d, the cube and dogbone-shaped specimens were used for compressive strength and uniaxial tension tests following the protocol in Table 5, where each test included 3 specimens per batch. Two linear variable displacement transducers (LVDT) were used to measure the tensile deformation of tensioned specimens.

For the self-healing and permeability tests, only the SS, DS-M0, and DS-M2 were examined as the other mixes DS-M2' and DS-M4 did not show significant advantages in crack width over DS-M0.

2.3. Self-healing tests

ECC has demonstrated autogenous healing ability due to its intrinsically tight crack width together with the presence of unhydrated cement grains [10,64]. However, the relatively larger crack width in PE/PP-ECC (due to the hydrophobic nature of these fibers) compromises the self-healing ability compared to ECC employing hydrophilic PVA fibers. To counteract this tendency, ML300D was utilized to promote the self-healing robustness of DS-ECC.

Fig. 4 shows the experimental process of self-healing test. Dogbone-shaped specimens of SS, DS-M0, and DS-M2 were pre-tensioned to 1 % and 2 % strain levels after 28 d of curing to induce damage, while virgin specimens (named 0 %) were adopted as a reference. The pre-cracked specimens were cured in two environmental conditions, i.e., 28 d of air curing (named as W/O heal condition) and 14 cycles of wet-dry curing comprising 24-h water immersion and 24-h air drying in each cycle (named as heal condition). After 14 wet-dry cycles/28 d air curing, the specimens were re-tested under uniaxial tension until failure to evaluate the recovery of tensile properties upon self-healing.

The resonant frequency (RF) technique has been proven to be a relatively simple gauge of material damage and degree of healing [10,65]. Fig. 5 depicts the protocol of RF measurement according to ASTM C215 [66]. The dogbone-shaped specimen was placed on a rubber plate and impacted by a needle hammer vertically onto the red dot as shown in Fig. 5. The sensor monitored the signals generated by the impact, and the RF was calculated by the resonance tester (Olson, model RT-1). Both the virgin specimens and cracked specimens were measured before each wet cycle (i.e. after each dry cycle).

A "*Normalized RF*" is proposed to measure the *RF* recovery degree and is calculated by the following equation:

$$Normalized\ RF_n = \frac{RF_n}{RF_{virgin}} \times 100\% \quad (1)$$

where RF_n is the RF of the healed specimen at cycle n, and RF_{virgin} is the RF of the virgin specimen at 28d (of air curing).

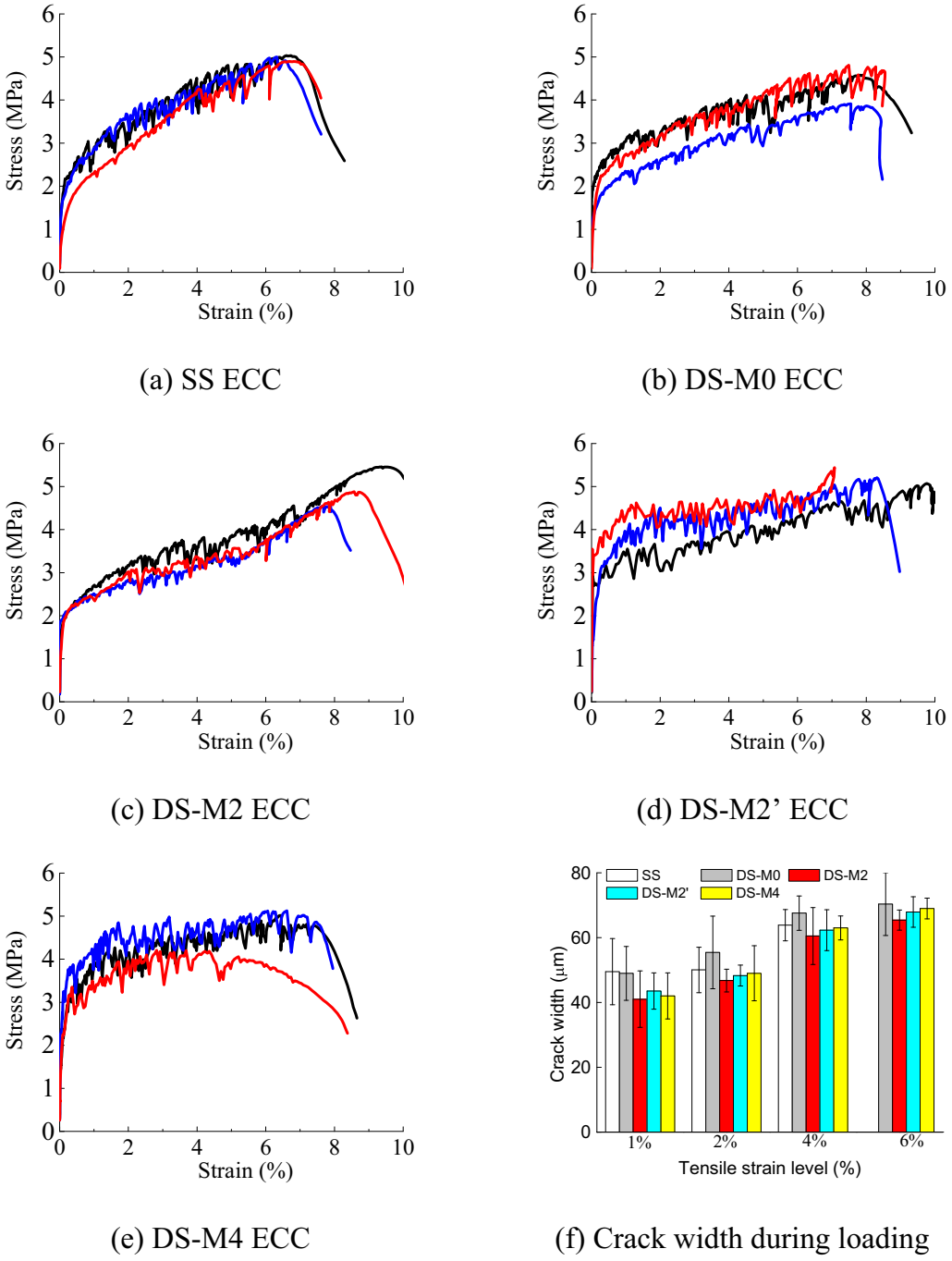

Fig. 7. Tensile performances of ECCs at 28 d.

2.4. Permeability tests

Water tightness is a critical performance to determine the suitability of ECC for water infrastructures and also represents resistance to the transport of aggressive agents through cracks. The dogbone specimens of DS-M0 and DS-M2 were pre-tensioned to 1 % and 2 % strain levels at 28 d, denoted as DS-M0-1%, DS-M0-2%, DS-M2-1%, and DS-M2-2%. Then the cracked specimens were placed horizontally in a falling head setup (Fig. 6) to measure the permeability of DS-ECC under a hydraulic gradient, as suggested by Lepech and Li [9]. The edges of the specimen were sealed with silicone sealant. Due to the long period of permeability tests, the pre-cracked specimens were conducted in an unloaded state. Monitoring of the coefficient of permeability (*CoP*) started 2 h after the specimens' seal and lasted 28 d, i.e. from the age of 28 d to 56 d. The *CoP* was calculated using Eq. (2).

$$CoP = \frac{a}{A}\frac{b}{t_f} ln\left(\frac{h_0}{h_f}\right) \tag{2}$$

where the notations' meaning and value are:

a is the cross-sectional area of the standpipe (2.84×10^{-5} m^2);
A is the cross-sectional area subject to flow (1.78×10^{-2} m^2);
b is the specimen thickness in the direction of flow (12.7 mm);
t_f is the test duration (measured during the test);
h_0 is the initial hydraulic head (measured during the test);
h_f is the final hydraulic head (measured during the test) at the time t_f.

Table 6
Summary of compressive and tensile results of ECCs.

Mixture	Compressive strength (MPa)	Ultimate tensile strength (MPa)	Tensile strain capacity (%)	Crack No.	Crack width[a] (μm)
SS	36.1	5.0	5.0	62	85
DS-M0	29.5	4.4	7.6	85	70
DS-M2	31.6	5.0	8.6	100	63
DS-M2'	28.5	5.2	8.4	84	74
DS-M4	35.5	4.8	6.1	73	69

[a] Crack width = Tensile strain capacity × (gauge length/crack number within gauge).

2.5. Chemical and microstructural characterizations

5-mm chunk samples of SS, DS-M0, DS-M2, and DS-M4 were extracted from the middle part of the dogbone specimen (green part in Fig. 3) at 28 d. Micromeritics AutoPore V Mercury Porosimeter was used to perform the pore structure analysis. Three chunk samples were placed in one sample cell and tested to obtain an average porosity [67]. The mercury contact angle was assumed as 130° [68]. Powders from grounded chunk samples passing a 75 μm sieve were used for the XRD test on a Rigaku Ultima IV instrument. Besides the ECC samples, ML300D powders mixed with an equal mass of water (named ML300D-water) were cast in a sealed vial. The ML300D-water sample was examined under XRD and SEM (Model: JEOL JSM-7800FLV) to analyze the hydration product of ML300D itself. At 28 d, all samples were fully immersed in isopropanol for 7 d, and then dried in a vacuum desiccator. In addition, the samples of DS-M0-heal and DS-M2-heal were prepared for the XRD test after 14 cycles of healing. Finally, ML300D-water powder, DS-M0-heal, and DS-M2-heal were examined under SEM to observe the healing products.

3. Experimental results and discussions

3.1. Compressive and uniaxial tensile performance

3.1.1. The effect of desert sand on mechanical performance

Desert sand ECC retains ultra-high ductility and strain-hardening performance similar to conventional silica sand ECC (Fig. 7). The ultimate tensile strength of DS-M0-ECC (4.4 MPa) is slightly lower than that of SS-ECC (5.0 MPa). Similarly, the compressive strength of DS-M0-ECC decreases to 29.5 MPa, compared to 36.0 MPa for SS-ECC. Despite a reduced compressive strength, the weakened matrix facilitates microcrack initiation, resulting in more cracks and a high tensile strain capacity. Table 6 lists the tensile results of ECC compositions, showing that DS-M0-ECC has a 7.6 % of tensile strain capacity and 85 cracks (within the 80 mm gauge length) at failure, which are higher than those of SS-ECC (5.0 % strain capacity and 62 cracks). The comparable properties of SS-ECC and DS-M0-ECC suggest the feasibility of developing ductile DS ECC.

The particle size dimension, morphology, and chemical compositions of desert sand contribute to the strength reduction of DS-M0 ECC. Desert sand has a wider particle range compared to silica sand (Fig. 2), where the larger sand could increase the air entrained into the matrix [24,28]. Further, the larger weak sand/paste interfaces represent larger flaws that suppress the compressive strength. In addition, the relative roundedness of desert sand (observed in Fig. 1) reduces the mechanical bonding between sand and matrix, leading to a decreased compressive strength, which has been reported in both concrete [25] and ECC [29]. Moreover, the SEM-EDS results (Fig. 1) suggest the presence of Ca, Al, Fe, and Mg, in addition to Si and O of silica sand, which may affect the hydration and strength gain. Although desert sand places a limit on the compressive and tensile strengths, the weakened matrix cracking strength actually improves the multiple cracking and crack width control by being more able to meet the composite multiple cracking criteria [4,69].

3.1.2. Capillary admixture effect

With the addition of the crystalline capillary waterproofing admixture (ML300D), DS-M2-ECC increases the compressive strength and ultimate tensile strength to 31.6 MPa and 5.0 MPa (Table 6). Moreover, DS-M2 possesses 8.6 % tensile strain capacity and more saturated microcracking (100 within gauge length) at failure, showing advantages over SS-ECC and DS-M0-ECC. Further, DS-M4 with double the ML300D admixture dosage improves the compressive strength to 35.5 MPa. However, the ultimate tensile strength (4.8 MPa) and ductility (6.1 %) are slightly compromised. The increased compressive strength is accompanied by an enhanced first cracking strength of DS-M4 (Fig. 7 (e)), which is related to the small flaw size/ finer pore size contributed by the admixture ML300D. DS-M4 has 73 cracks at failure with 69 μm of average crack width, exhibiting a less saturated crack pattern compared to DS-M2 (Fig. 8). Thus, 2 % binder weight of ML300D is chosen as the optimal dosage for the DS-ECC in this study, possessing the highest ultimate tensile strength, ductility, and crack numbers, but with the lowest

(a) SS (b) DS-M0 (c) DS-M2 (d)DS-M2' (e) DS-M4

Fig. 8. Crack pattern within the 80 mm gauge length of ECCs after tensile failure.

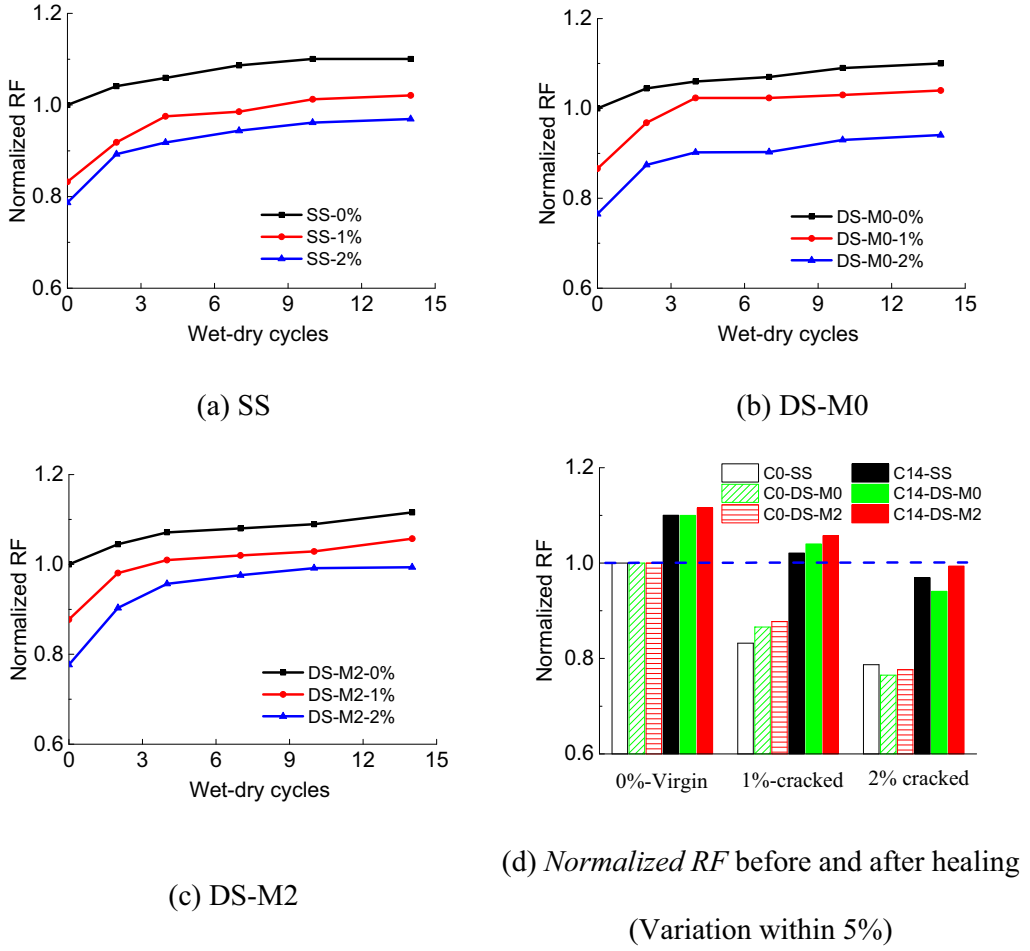

Fig. 9. Resonant frequency recovery with wet-dry cycles.

crack width.

3.1.3. *Crumb rubber effect*

Crumb rubber (CR) was utilized as artificial flaws to initiate the cracks, which further control the crack width for robust self-healing performance. Two dosages (30 g/L and 60 g/L) were adopted to tailor the crack pattern and ductility. DS-M2' displays a lower compressive strength (28.5 MPa) but a comparable tensile strength to DS-M2 with 30 g/L CR. Although CR can facilitate crack initiation, excess CR would cause dispersion issues, leading to the aggregation of CR particles. Consequently, local failure and unsaturated cracks may occur, accounting for the reduced crack number of DS-M2' (84 cracks) compared to that 100 cracks of DS-M2 (Table 6 and Fig. 8). Although the crack width distribution in Fig. 7(f) shows some variations within 10 μm, the crack width for DS-M2' is higher than that of DS-M2, consistent with observations in previous studies [70,71]. Adding to cost concerns, 30 g/L of crumb rubber is adopted for specimens used in the self-healing and permeability tests.

3.2. *Self-healing ability*

Since DS-M2 has been demonstrated with tiny cracks and ultra-high ductility, the self-healing and permeability performance of DS-M2 were studied. SS and DS-M0 served as benchmarks.

3.2.1. *Resonant frequency results of the healed specimens*

Resonant frequency (*RF*) was utilized as an indicative measure of the recovery extent of deliberately damaged DS-ECCs after exposure to wet-dry cycles. Virgin specimen (0 % preloading) experiences an increase in the normalized RF to approximately 110 % after 14 wet-dry cycles (Fig. 9) due to continuing hydration of the bulk material. For the pre-cracked specimens prior to healing (denoted as C0), the normalized RF drops to 80–85 % for 1 % pre-cracked specimens and to 75–80 % for 2 % pre-cracked specimens. Most of the RF recovery occurs in the first 5 wet-dry cycles, consistent with previous findings [38]. All three mixtures gain a full RF recovery after 1 % imposed strain. Moreover, DS-M2 shows a slightly higher recovery than SS and DS-M0. Specifically, DS-M2 attains 99 % RF recovery after 14 cycles compared to 94 % for DS-M0, at 2 % pre-load strain level.

The evolution of crack appearance in Figs. 10–12 further verifies the healing ability of ECCs. SS-ECC and DS-M0-ECC show a similar healing trend, i.e., cracks under 20 μm are filled by healing products (Figs. 10(a) and 11(a)). Partial healing is observed (Figs. 10(b) and 11(b)) for cracks with 20–30 μm width, while negligible healing is found when crack width exceeds 40 μm (Figs. 10(c) and 11(c)). Most crack healings are attained before the 7th cycle and show little change after that, which is consistent with the RF evolution process.

DS-M2 ECC exhibits a more robust healing ability compared to DS-M0 ECC and SS ECC. The crystalline admixture enables full healing of cracks up to 30–40 μm width (Fig. 12(a)). Cracks wider than 50 μm and even up to 80 μm (Fig. 12(b–c)) experience partial healing, suggesting that most cracks under 2 % of pre-loading can be healed autogenously in DS-M2 ECC.

3.2.2. *Recovery of tensile properties*

In addition to the studies on RF recovery and crack appearance, the

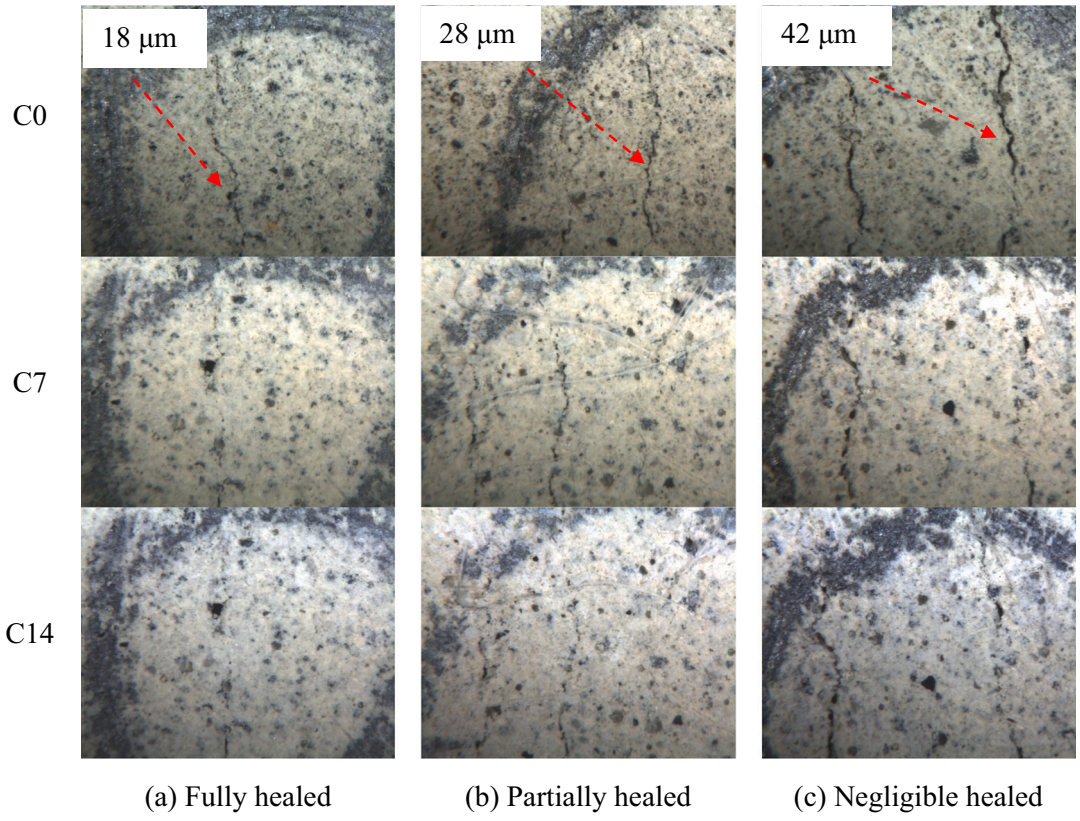

Fig. 10. Optical micrographs of crack evolution with wet-dry cycles of SS ECC.

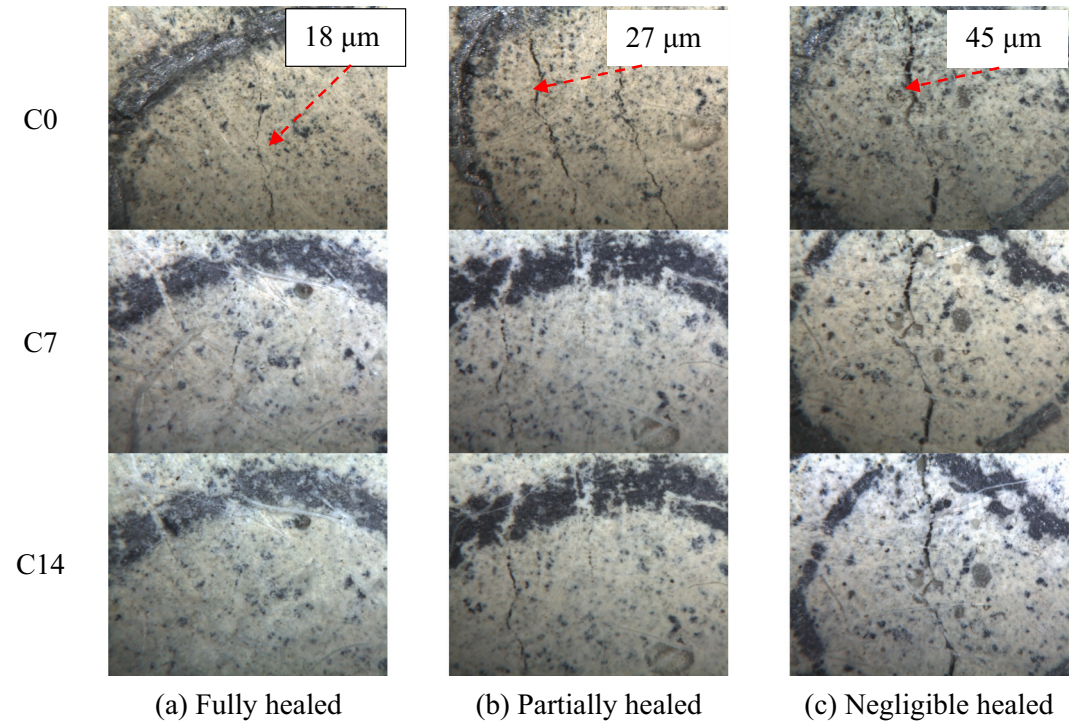

Fig. 11. Optical micrographs of crack evolution with wet-dry cycles of DS-M0 ECC.

mechanical performance under tension of healed specimens was investigated (Figs. 13–15). DS ECC shows a similar stress-strain relationship to that of SS ECC. Regardless of mixtures, the virgin specimens show a negligible change in tensile strength without self-healing (W/O heal under air-curing) but a significant tensile strength gain after wet-dry cycles. Decays of both tensile strength and ductility are observed for the 1 %/2 % pre-cracked specimens under air curing conditions compared to that of 28d-Ref. However, these tensile properties are

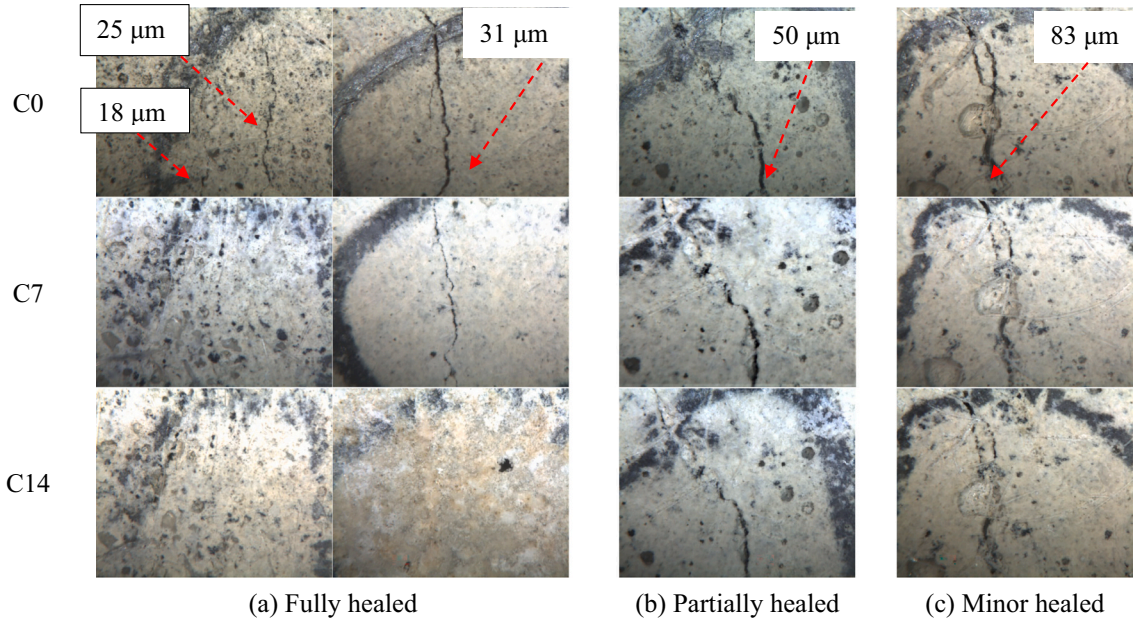

Fig. 12. Optical micrographs of crack evolution with wet-dry cycles of DS-M2. Cracks <31 mm-width are fully healed.

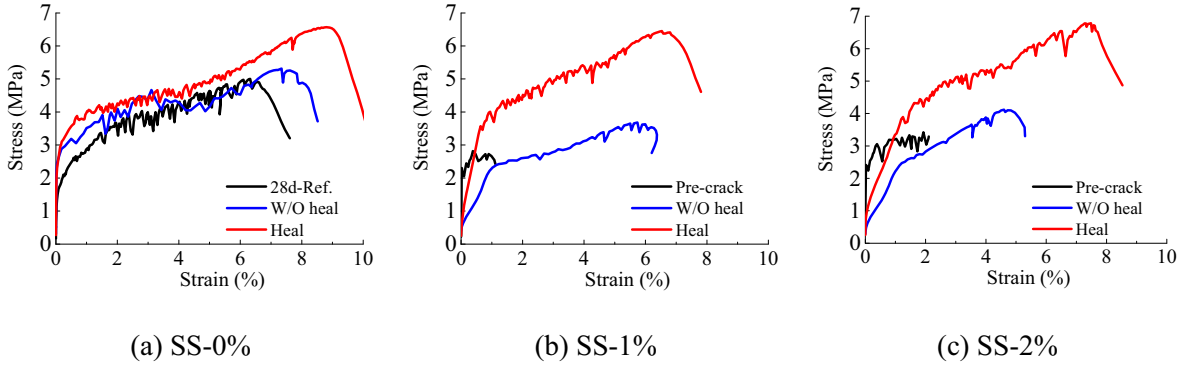

Fig. 13. The effect of healing on the tensile stress-strain relationship of SS ECC.

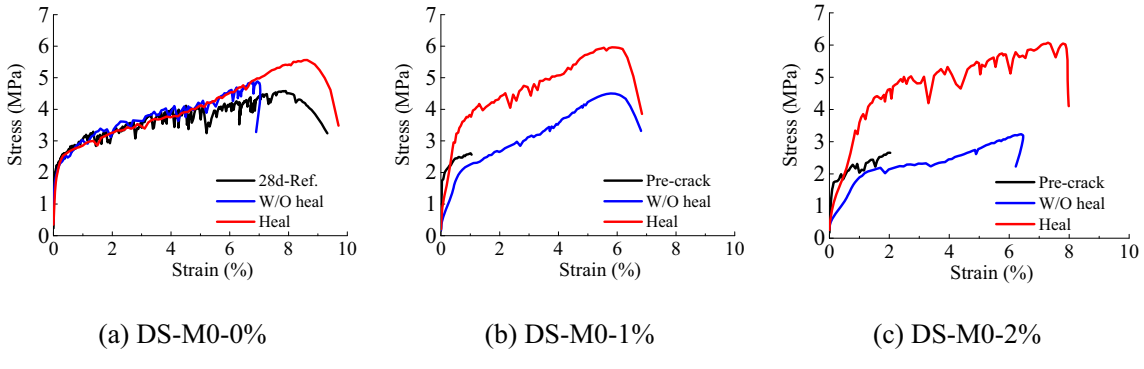

Fig. 14. The effect of healing on the tensile stress-strain relationship of DS-M0 ECC.

recovered after 14 wet-dry cycles, where the ultimate tensile strength of cracked specimens is higher than the virgin specimens at 28 d and almost identical to the strength of virgin specimens after 14 wet-dry cycles.

Tensile stiffness/modulus can be expressed by the relative variation ratio of tensile stress and tensile strain, which is intuitively shown as the slope of tensile stress-strain curves during the elastic stage (before strain-hardening). Figs. 13–15 show that the tensile stiffness of pre-cracked ECC without healing is considerably reduced. Although tensile stiffness has been improved to a great extent after 14 cycles of wet-dry conditioning, it remains lower than the virgin specimen. The relatively low magnitude of tensile strain will result in a large calculated error, yielding a large variation in the calculated stiffness from the tensile stress-strain curves, hence, the stiffness recovery is not quantitatively

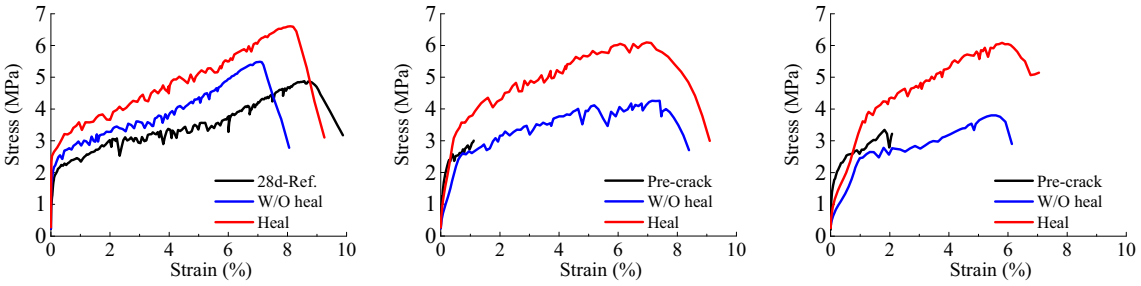

(a) DS-M2-0% (b) DS-M2-1% (c) DS-M2-2%

Fig. 15. The effect of healing on the tensile stress-strain relationship of DS-M2 ECC.

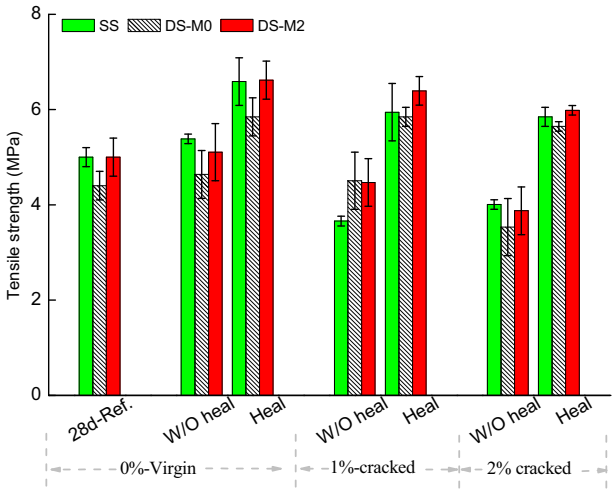

Fig. 16. Ultimate tensile strength of ECCs with and without healing.

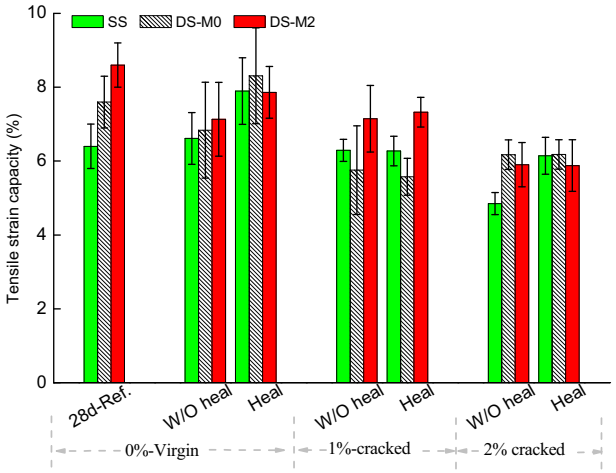

Fig. 17. Tensile strain capacity of ECCs with and without healing.

compared among mixtures (SS, DS-M0, DS-M2). However, all mixtures show a stiffness recovery to a level between those of the virgin specimens and W/O healed specimens. As expected, the 1 % pre-strained specimens have a larger stiffness recovery than that of the 2 % pre-strained specimens.

Figs. 16–17 summarize the tensile strength and ductility of ECCs with and without healing. For all pre-tensioned levels, DS-M0 ECC shows a lower tensile strength than SS ECC for both healed and W/O healed conditions. DS-M2 improves the tensile strength of ECC, especially for the cracked specimen after healing, the ultimate tensile strength is slightly higher than that of SS ECC. Also, the healed pre-tensioned specimens display a significantly higher tensile strength than the 28d-Ref. and comparable tensile strength to the healed virgin specimen (around 6 MPa). In contrast with strength results, all mixtures after healing show diminished ductility. However, DS-M2 maintains 7.0 % and 6.3 % of tensile strain capacity after 1 % and 2 % pre-straining, respectively, which remains much higher than traditional ECC (3 %–5 % of ductility).

3.3. Permeability test results

The crack width just after loading determines the initial permeability performance of ECC. Due to autogenous self-healing, the long-term coefficient of permeability (*CoP*) of ECC is significantly reduced. Fig. 18 compares the permeability evolutions of DS-M0 and DS-M2. DS-M0-1% has a lower *CoP* than DS-M0-2% from 28 d to 56 d. DS-M2-1% and DS-M2-2% have comparable *CoP* evolution. Due to the tiny crack width of DS-M2, the initial *CoP* of DS-M2-1% (1.6×10^{-8} m/s) is smaller than that of DS-M0-1% (2.6×10^{-8} m/s). Under 2 % imposed strain, the initial *CoP* of DS-M2 (3.6×10^{-8} m/s) is 55 % that of DS-M0 (6.5×10^{-8} m/s). Furthermore, due to the intrinsic self-healing ability of ECC, the *CoP* of DS-M0-1% decreases to 6.2×10^{-10} m/s magnitude after 28 days of water immersion, while DS-M0-2% shows 1.3×10^{-9} m/s magnitude. In contrast, DS-M2-2% attains a long-term *CoP* of 3.9×10^{-10} m/s, comparable to that of conventional M45-PVA-ECC [9].

The excellent water tightness of DS-M2 can be explained by the sealing of cracks by healing products. Fig. 19 presents the DS-M0 ECC and DS-M2 ECC specimens after permeability tests. DS-M2-2% shows obvious healing of cracks compared to partial healing of cracks in DS-M0-2%. Precipitation of hydration products results in a robust self-healing ability and a concomitant reduction in crack permeability. Therefore, the water-proofing ability and durability of ECC are demonstrated in ECC utilizing desert sand and ML300D admixture (DS-M2).

3.4. Micro/chemical analysis

3.4.1. Pore structure

Pore structure analysis demonstrates that desert sand tends to increase the composite porosity compared to the reference silica sand ECC. The inclusion of ML300D refines the pore structure. Fig. 20 depicts the differential and cumulative intruded mercury volume variation with pore diameter. DS-M0 ECC has a larger total intruded pore volume (1.90 mL/g) compare to that of SS ECC (1.74 mL/g). With the inclusion of 2 % binder weight of ML300D, DS-M2 shows a comparable total intruded pore volume to DS-M0, however, with finer pores. When the content of ML300D increased to 4 % binder weight, the cumulative volume (1.68 mL/g) was lower than that of SS ECC.

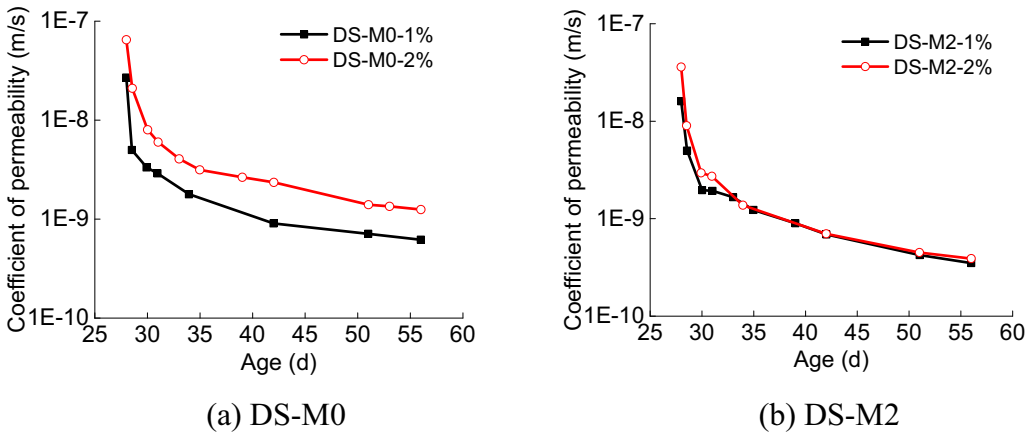

Fig. 18. The *CoP* evolution with time of DS ECCs.

Fig. 19. Crack appearance after permeability tests.

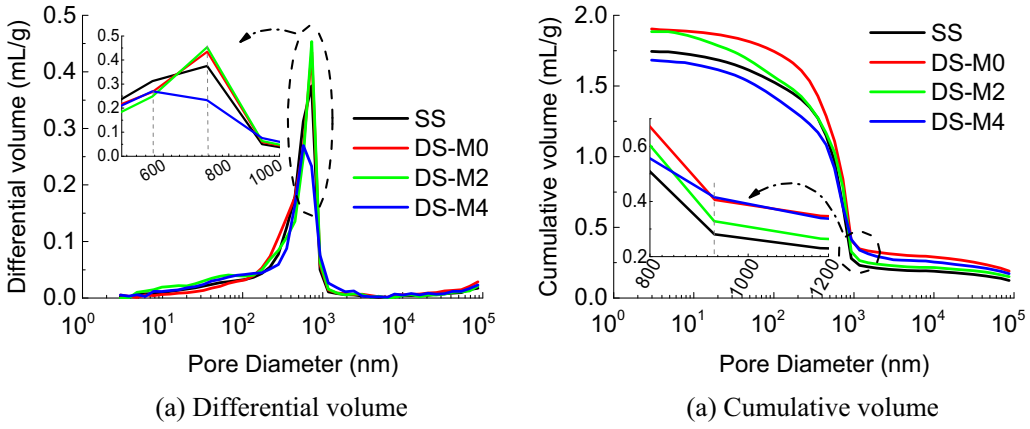

Fig. 20. Intruded volume of mercury with pore diameter distributions.

The pores were classified as gel pores (<10 nm), medium (10 nm–50 nm) and large (50 nm-10 μm) capillary pores, and air voids (>10 μm) in Fig. 21 [72,73], which have been identified as harmless, less-harmful, harmful, and more harmful pores depending on their effect on the strength and durability of concrete [74]. While gel and medium capillary pores influence shrinkage, the strength is mainly affected by air voids and large capillary pores [73]. More air voids are introduced by desert sand than silica sand, accounting for the compressive strength reduction in DS-M0 ECC (in comparison with SS ECC). DS-M2 ECC refines the gel and medium capillary pores, slightly improving the

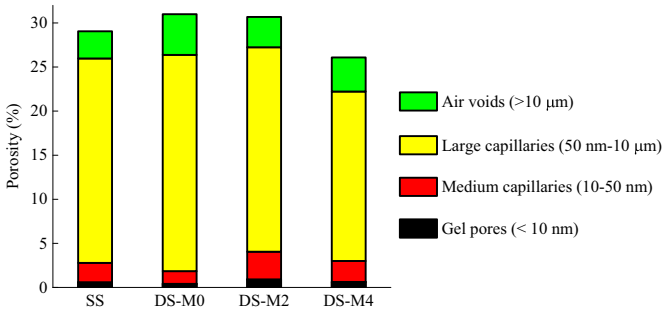

Fig. 21. The porosity distribution with different pore structures.

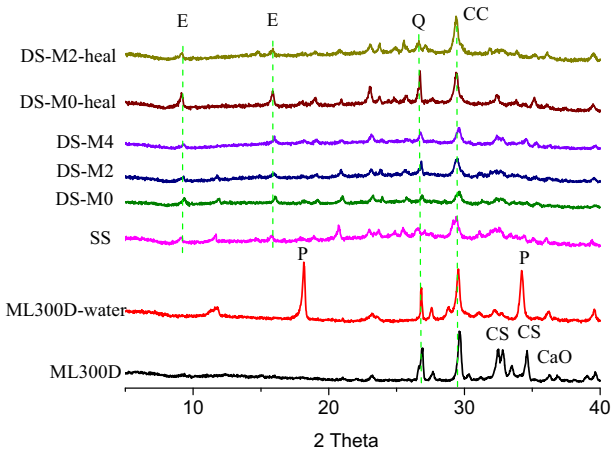

Fig. 22. XRD patterns of the ML300D and ECCs.
(E: ettringite, P: portlandite (CH), Q: quartz, CC: calcite, CS: calcium silicates).

compressive strength of DS-M2 ECC to 31.6 MPa. DS-M4 further refines the large capillary pores and restores the compressive strength to 35.5 MPa. The additional C-S-H gel and CH produced by the hydration of ML300D contribute to the pore structure and strength improvements, which is further demonstrated in the XRD results (Section 3.4.2).

Although desert sand increases the total porosity and ML300D refines the pore structure, neither has significant effects on the critical pore diameter and threshold pore diameter. The critical pore diameter corresponds to the peak value in the differential volume curve and the threshold can be determined by the turning point on the cumulative volume curve (Fig. 20) [72]. The insignificant change of critical and threshold pore diameter implies that the permeability of uncracked SS ECC, DS-M0 ECC, and DS-M2 ECC are comparable to each other as noted above.

Besides desert sand and ML300D, the presence of fibers significantly affects the critical pore diameters. As reported in a previous study [75], PVA fibers have less influence on the porosity and critical diameter. However, due to the larger quantities of PE/PP fibers associated with their smaller diameter than PVA fibers, longer mixing time and higher mixing speed are required for PE/PP ECC, leading to more entrained air in the matrix. Consequently, the critical pore diameter of DS-M2 (727 nm) is coarser than that in ECC composition with PVA fibers (12 nm) [75].

3.4.2. *Chemical analysis*

XRD results (Fig. 22) suggest that the desert sand and ML300D do not change the mineral compositions of the hydration products. That is, SS, DS-M0, DS-M2, and DS-M4 ECC have similar hydration products, where the ettringite is primarily produced by CSA cement, and quartz is mainly introduced by sand. Since the ECC samples were cured in air, minor calcite (CC) may be generated by the reaction of CO_2 and CH. Regarding

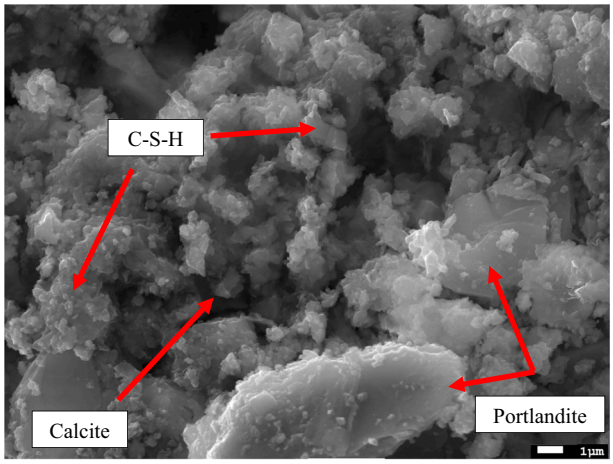

(a) ML300D-water.

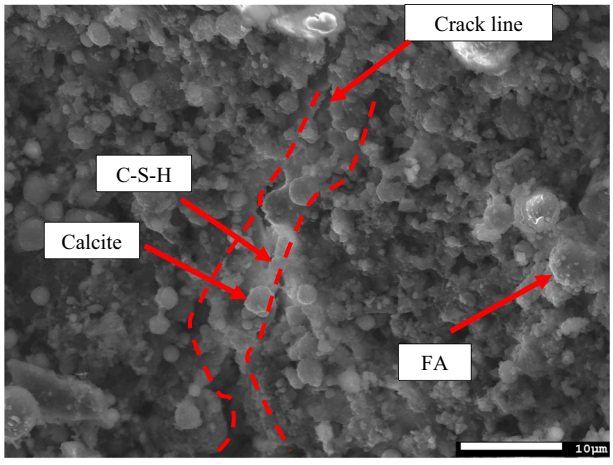

(b) DS-M0-heal.

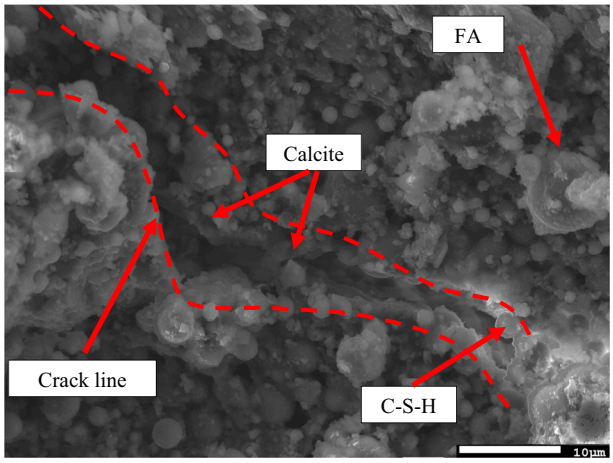

(c) DS-M2-heal.

Fig. 23. SEM results (Working Distance = 10 mm, Voltage = 15 kV, Current = 12 A).

the healed samples, more calcite can be observed for DS-M0-heal and DS-M2-heal compared to the samples cured in air. No significant difference in the healing products between DS-M0-heal and DS-M2-heal are found. The limestone filler in ML300D (Fig. 22) provides more nucleation sites, facilitating the precipitation of CH [76]. As a result, ML300D-water shows plenty of CH in its XRD pattern, which is also observed in

SEM (Fig. 23(a)). The hydration product CH boosts the precipitation of calcite and improves the healing degree of DS-M2 ECC.

Besides the CH, calcium-silicate-hydrate (C-S-H) is also observed in the SEM picture (Fig. 23(a)), showing the hydration products of ML300D and water. Fig. 23(a) suggests ML300D can react with water to produce C-S-H, which further supports the finding that DS-M2 has finer pore structures. The healing products, mainly calcite and C-S-H, are observed along the crack lines in both DS-M0-heal and DS-M2-heal (Fig. 23), which is consistent with the XRD results and previous studies [36,38]. The C-S-H can be produced from the hydration of both OPC and ML300D.

As confirmed by the SEM and XRD results, the crystalline admixture (ML300D) reacts with water to produce additional CH and C-S-H gel, which refines the micropores and contributes to the improvement of strength (Section 3.1.2). In addition, the generated CH provides more Ca^{2+} along the crack lines, enhancing the precipitation of calcium carbonate, which boosts the self-healing capacity. The self-healed ECC possesses a reduced permeability and improved mechanical properties recovery. The inclusion of crystalline admixture further enhanced the healing capacity robustness of the developed ECC.

4. Conclusions

A durable ECC has been developed using locally available materials, including desert sand, crumb rubber, and PE/PP fibers. A commercial crystalline capillary waterproofing admixture (MasterLife 300D) was included to enhance mechanical and self-healing performance. Multi-scaled analyses have been conducted, including materials properties testing (compressive/tensile tests, self-healing, and permeability tests) and micro/chemical analyses (MIP, XRD, SEM). Based on the experimental results, the following conclusions can be drawn:

- When manufactured silica sand is replaced by desert sand, the compressive and tensile strength of the resulting ECC are reduced (by 18 % and 12 %, respectively) due to the round morphology, larger particle size, and impurities intrinsic in the desert sand. On the positive side, the weakened matrix and fracture toughness facilitate microcrack initiation and multiple steady-state cracks, resulting in improved ductility and crack width for desert sand ECC (DS-M0).
- The compromised strength was found restorable by the addition of crystalline admixture (MasterLife 300D). 2 % binder weight of MasterLife 300D (DS-M2) is chosen as the optimal dosage for this study. DS-M2 shows enhanced tensile performance and saturated crack pattern compared with DS-M0. Specifically, DS-M2 ECC attains an ultimate tensile strength of 5.0 MPa, tensile strain capacity of 8.6 %, and crack width below 63 μm at 28 d, placing this composition as having the highest ductility and lowest crack width among the desert sand ECCs published in the literature. The compressive strength of DS-M2 is 31.6 MPa.
- Crystalline admixture produces additional C-S-H gel and crystalline $Ca(OH)_2$ precipitates, endowing the desert sand ECC with enhanced healing ability. DS-M2 demonstrates a robust autogenous healing ability under conditions of wet-dry cycles and water immersion. DS-M2 recovers 99 % of resonant frequency under 2 % imposed strain, compared to 94 % for DS-M0. In addition, remarkable restored tensile mechanical properties of pre-damaged DS-M2 after wet-dry curing were attained. Specifically, 2 % pre-strained DS-M2 specimens recovered a tensile strength of 6 MPa, 20 % higher than the virgin specimen at 28 d (5 MPa) and comparable to that of the virgin specimen after 14 wet-dry curing cycles.
- The developed desert sand ECC has the capacity of healing cracks with larger widths. While DS-M0 can only fully heal cracks with a width below 20 μm, crack width between 30 and 40 μm can be fully healed in DS-M2. Partial healing is also observed for cracks with a width larger than 50 μm and even up to 80 μm.
- The superior crack control performance of DS-M2 leads to a lower initial coefficient of permeability (*CoP*). The enhanced self-healing ability results in an even smaller long-term *CoP*. Specifically, the initial and long-term *CoP* of DS-M2 with 2 % pre-straining are 3.6×10^{-8} m/s and 3.9×10^{-10} m/s, respectively.

The ultra-high ductility (8.6 %), tiny crack width (63 μm at failure), and robust self-healing ability of the developed desert sand ECC represent a durable ECC using local ingredients. These characteristics hold promise in applications in new construction and in rehabilitating aging infrastructures in regions where desert sand is plentiful.

CRediT authorship contribution statement

He Zhu: Conceptualization, Methodology, Investigation, Formal analysis, Roles/Writing - original draft; Writing - review & editing.
Yichao Wang: Investigation, Review.
Mohammed Mehthel: Investigation, Review.
Thibault Villette: Investigation, Review.
Oscar Salazar VIDAL: Investigation, Review.
Waleed N. Nasser: Investigation, Review.
Victor C. Li: Funding acquisition, Project administration, Conceptualization, Writing - Review & Editing.

Declaration of competing interest

The authors declare that they have no known competing financial interests or personal relationships that could have appeared to influence the work reported in this paper.

Data availability

Data will be made available on request.

Acknowledgments

This research is supported by a research grant (Contract SATC 2020-004) from Saudi Aramco Technologies Company to the University of Michigan. The authors acknowledge the materials supply from BASF Chemicals company (MasterLife 300D), Entech Inc. (crumb rubber), and CTS Cement Manufacturing Corporation (CSA cement).

References

[1] M.F. Ashby, Materials and the Environment: Eco-Informed Material Choice, 2nd ed., Elsevier, 2012.
[2] E. Benhelal, E. Shamsaei, M.I. Rashid, Challenges against CO2 abatement strategies in cement industry: a review, J. Environ. Sci. 104 (2021) 84–101, https://doi.org/10.1016/J.JES.2020.11.020.
[3] P.J.M. Monteiro, S.A. Miller, A. Horvath, Towards sustainable concrete, Nat. Mater. 16 (2017) 698–699, https://doi.org/10.1038/nmat4930.
[4] V.C. Li, Engineered cementitious composites (ECC), Springer, 2019, https://doi.org/10.1007/978-3-662-58438-5.
[5] H. Zhu, Y. Hu, R. Ma, J. Wang, Q. Li, Concrete thermal failure criteria , test method , and mechanism: a review, Constr. Build. Mater. 283 (2021), 122762, https://doi.org/10.1016/j.conbuildmat.2021.122762.
[6] H. Zhu, Y. Hu, Q. Li, R. Ma, Restrained cracking failure behavior of concrete due to temperature and shrinkage, Constr. Build. Mater. 244 (2020), https://doi.org/10.1016/j.conbuildmat.2020.118318.
[7] H. Zhu, T. Wang, Y. Wang, V.C. Li, Trenchless rehabilitation for concrete pipelines of water infrastructure: a review from the structural perspective, Cem. Concr. Compos. 123 (2021), 104193, https://doi.org/10.1016/j.cemconcomp.2021.104193.
[8] H. Liu, Q. Zhang, C. Gu, H. Su, V. Li, Influence of microcrack self-healing behavior on the permeability of engineered cementitious composites, Cem. Concr. Compos. 82 (2017) 14–22, https://doi.org/10.1016/j.cemconcomp.2017.04.004.
[9] M.D. Lepech, V.C. Li, Water permeability of engineered cementitious composites, Cem. Concr. Compos. 31 (2009) 744–753, https://doi.org/10.1016/j.cemconcomp.2009.07.002.
[10] H. Zhu, D. Zhang, T. Wang, H. Wu, V.C. Li, Mechanical and self-healing behavior of low carbon engineered cementitious composites reinforced with PP-fibers, Constr.

Build. Mater. 259 (2020), 119805, https://doi.org/10.1016/j.conbuildmat.2020.119805.
[11] H. Zhu, D. Zhang, T. Wang, V.C. Li, Intrinsic self-stressing and low carbon engineered cementitious composites (ECC) for improved sustainability, Cem. Concr. Res. 149 (2021), 106580, https://doi.org/10.1016/j.cemconres.2021.106580.
[12] E.H. Yang, Y. Yang, V.C. Li, Use of high volumes of fly ash to improve ECC mechanical properties and material greenness, ACI Mater. J. 104 (2007) 620–628, https://doi.org/10.14359/18966.
[13] Z. Zhang, F. Yang, J.C. Liu, S. Wang, Eco-friendly high strength, high ductility engineered cementitious composites (ECC) with substitution of fly ash by rice husk ash, Cem. Concr. Res. 137 (2020), 106200, https://doi.org/10.1016/j.cemconres.2020.106200.
[14] K.Q. Yu, W.J. Zhu, Y. Ding, Z.D. Lu, J. Tao Yu, J.Z. Xiao, Micro-structural and mechanical properties of ultra-high performance engineered cementitious composites (UHP-ECC) incorporation of recycled fine powder (RFP), Cem. Concr. Res. 124 (2019), 105813, https://doi.org/10.1016/J.CEMCONRES.2019.105813.
[15] X. Huang, R. Ranade, V.C. Li, Feasibility study of developing green ECC using iron ore tailings powder as cement replacement, J. Mater. Civ. Eng. 25 (2013) 923–931, https://doi.org/10.1061/(asce)mt.1943-5533.0000674.
[16] L. Li Kan, R. Xin Shi, J. Zhu, Effect of fineness and calcium content of fly ash on the mechanical properties of Engineered Cementitious Composites (ECC), Constr. Build. Mater. 209 (2019) 476–484, https://doi.org/10.1016/j.conbuildmat.2019.03.129.
[17] S. Wang, V.C. Li, Engineered cementitious composites with high-volume fly ash, ACI Mater. J. 104 (2007) 233–241, https://doi.org/10.14359/18668.
[18] Y. Li, X. Guan, C. Zhang, T. Liu, Development of high-strength and high-ductility ECC with saturated multiple cracking based on the flaw effect of Coarse River sand, J. Mater. Civ. Eng. 32 (2020) 04020317, https://doi.org/10.1061/(asce)mt.1943-5533.0003405.
[19] B.T. Huang, J.Q. Wu, J. Yu, J.G. Dai, C.K.Y. Leung, V.C. Li, Seawater Sea-sand engineered/strain-hardening cementitious composites (ECC/SHCC): assessment and modeling of crack characteristics, Cem. Concr. Res. 140 (2021), 106292, https://doi.org/10.1016/J.CEMCONRES.2020.106292.
[20] M. Sahmaran, M. Lachemi, K.M.A. Hossain, R. Ranade, V.C. Li, Influence of aggregate type and size on ductility and mechanical properties of engineered cementitious composites, ACI Mater. J. 106 (2009) 308–316, https://doi.org/10.14359/56556.
[21] X. Guan, Y. Li, T. Liu, C. Zhang, H. Li, J. Ou, An economical ultra-high ductile engineered cementitious composite with large amount of coarse river sand, Constr. Build. Mater. 201 (2019) 461–472, https://doi.org/10.1016/J.CONBUILDMAT.2018.12.207.
[22] J. Xiao, C. Qiang, A. Nanni, K. Zhang, Use of sea-sand and seawater in concrete construction: current status and future opportunities, Constr. Build. Mater. 155 (2017) 1101–1111, https://doi.org/10.1016/J.CONBUILDMAT.2017.08.130.
[23] A.S. Al-Harthy, M.A. Halim, R. Taha, K.S. Al-Jabri, The properties of concrete made with fine dune sand, Constr. Build. Mater. 21 (2007) 1803–1808, https://doi.org/10.1016/J.CONBUILDMAT.2006.05.053.
[24] F.J. Luo, L. He, Z. Pan, W.H. Duan, X.L. Zhao, F. Collins, Effect of very fine particles on workability and strength of concrete made with dune sand, Constr. Build. Mater. 47 (2013) 131–137, https://doi.org/10.1016/j.conbuildmat.2013.05.005.
[25] E.S.S.A. Seif, Assessing the engineering properties of concrete made with fine dune sands: An experimental study, Arab. J. Geosci. 6 (2013) 857–863, https://doi.org/10.1007/s12517-011-0376-6.
[26] X. An, J. Che, H. Liu, S. Yang, S.I. Doh, Study on freeze-thaw resistance with NaCl of desert sand engineering cement composites, Phys. Chem. Earth, Parts A/B/C. 121 (2021), 102954, https://doi.org/10.1016/J.PCE.2020.102954.
[27] W. Yan, G. Wu, Z. Dong, Optimization of the mix proportion for desert sand concrete based on a statistical model, Constr. Build. Mater. 226 (2019) 469–482, https://doi.org/10.1016/J.CONBUILDMAT.2019.07.287.
[28] S. Chuah, W.H. Duan, Z. Pan, E. Hunter, A.H. Korayem, X.L. Zhao, F. Collins, J. G. Sanjayan, The properties of fly ash based geopolymer mortars made with dune sand, Mater. Des. 92 (2016) 571–578, https://doi.org/10.1016/j.matdes.2015.12.070.
[29] H.L. Wu, J. Yu, D. Zhang, J.X. Zheng, V.C. Li, Effect of morphological parameters of natural sand on mechanical properties of engineered cementitious composites, Cem. Concr. Compos. 100 (2019) 108–119, https://doi.org/10.1016/J.CEMCONCOMP.2019.04.007.
[30] M. Iqbal Khan, G. Fares, S. Mourad, Optimized fresh and hardened properties of strain hardening cementitious composites: effect of mineral admixtures, cementitious composition, size, and type of aggregates, J. Mater. Civ. Eng. 29 (2017) 04017178, https://doi.org/10.1061/(asce)mt.1943-5533.0002039.
[31] D. Meng, T. Huang, Y.X. Zhang, C.K. Lee, Mechanical behaviour of a polyvinyl alcohol fibre reinforced engineered cementitious composite (PVA-ECC) using local ingredients, Constr. Build. Mater. 141 (2017) 259–270, https://doi.org/10.1016/j.conbuildmat.2017.02.158.
[32] J. Che, D. Wang, H. Liu, Y. Zhang, Mechanical properties of desert sand-based fiber reinforced concrete (DS-FRC), Appl. Sci. 9 (2019), https://doi.org/10.3390/app9091857.
[33] M.I. Khan, G. Fares, S. Mourad, W. Abbass, Optimized fresh and hardened properties of strain-hardening cementitious composites: effect of sand size and workability, J. Mater. Civ. Eng. 28 (2016) 04016152, https://doi.org/10.1061/(asce)mt.1943-5533.0001665.
[34] K. Yu, Y. Wang, J. Yu, S. Xu, A strain-hardening cementitious composites with the tensile capacity up to 8%, Constr. Build. Mater. 137 (2017) 410–419.
[35] B. Felekoglu, K. Tosun-Felekoglu, R. Ranade, Q. Zhang, V.C. Li, Influence of matrix flowability, fiber mixing procedure, and curing conditions on the mechanical performance of HTPP-ECC, Compos. Part B Eng. 60 (2014) 359–370, https://doi.org/10.1016/J.COMPOSITESB.2013.12.076.
[36] V.C. Li, E.-H. Yang, Self Healing in Concrete Materials, Self Heal. Mater., Springer, in, 2007, pp. 161–193.
[37] V. Cappellesso, D. di Summa, P. Pourhaji, N. Prabhu Kannikachalam, K. Dabral, L. Ferrara, M. Cruz Alonso, E. Camacho, E. Gruyaert, N. De Belie, A Review of the Efficiency of Self-Healing Concrete Technologies for Durable and Sustainable Concrete Under Realistic Conditions, 2023, https://doi.org/10.1080/09506608.2022.2145747.
[38] L.L. Kan, H.S. Shi, A.R. Sakulich, V.C. Li, Self-healing characterization of engineered cementitious composite materials, ACI Mater. J. 107 (2010) 617–624, https://doi.org/10.14359/51664049.
[39] L. Ferrara, V. Krelani, M. Carsana, A "fracture testing" based approach to assess crack healing of concrete with and without crystalline admixtures, Constr. Build. Mater. 68 (2014) 535–551, https://doi.org/10.1016/j.conbuildmat.2014.07.008.
[40] T. Chandra Sekhara Reddy, A. Ravitheja, C. Sashidhar, Micromechanical properties of self-healing concrete with crystalline admixture and silica fume, ACI Mater. J. 117 (2020) 63–74, https://doi.org/10.14359/51722395.
[41] J.Y. Wang, H. Soens, W. Verstraete, N. De Belie, Self-healing concrete by use of microencapsulated bacterial spores, Cem. Concr. Res. 56 (2014) 139–152, https://doi.org/10.1016/J.CEMCONRES.2013.11.009.
[42] K. Van Tittelboom, J. Wang, M. Araújo, D. Snoeck, E. Gruyaert, B. Debbaut, H. Derluyn, V. Cnudde, E. Tsangouri, D. Van Hemelrijck, N. De Belie, Comparison of different approaches for self-healing concrete in a large-scale lab test, Constr. Build. Mater. 107 (2016) 125–137, https://doi.org/10.1016/J.CONBUILDMAT.2015.12.186.
[43] Z. Zhang, Y. Ding, S. Qian, Influence of bacterial incorporation on mechanical properties of engineered cementitious composites (ECC), Constr. Build. Mater. 196 (2019) 195–203, https://doi.org/10.1016/J.CONBUILDMAT.2018.11.089.
[44] K. Vijay, M. Murmu, S.V. Deo, Bacteria based self healing concrete – a review, Constr. Build. Mater. 152 (2017) 1008–1014, https://doi.org/10.1016/j.conbuildmat.2017.07.040.
[45] Y.S. Lee, W. Park, Current challenges and future directions for bacterial self-healing concrete, Appl. Microbiol. Biotechnol. 102 (2018) 3059–3070, https://doi.org/10.1007/s00253-018-8830-y.
[46] B. Aytekin, A. Mardani, Ş. Yazıcı, State-of-art review of bacteria-based self-healing concrete: biomineralization process, crack healing, and mechanical properties, Constr. Build. Mater. 378 (2023), https://doi.org/10.1016/j.conbuildmat.2023.131198.
[47] A. de Souza Oliveira, J. Dweck, E. de Moraes Rego Fairbairn, O. da Fonseca Martins Gomes, R.D. Toledo Filho, Crystalline admixture effects on crystal formation phenomena during cement pastes' hydration, J. Therm. Anal. Calorim. 139 (2020) 3361–3375, https://doi.org/10.1007/s10973-019-08745-0.
[48] K. Sisomphon, O. Copuroglu, E.A.B. Koenders, Self-healing of surface cracks in mortars with expansive additive and crystalline additive, Cem. Concr. Compos. 34 (2012) 566–574, https://doi.org/10.1016/J.CEMCONCOMP.2012.01.005.
[49] F. Martins, L. Ferrara, A. De Souza, E. De Moraes, R. Fairbairn, R. Dias, T. Filho, An overview of a twofold effect of crystalline admixtures in cement-based materials: from permeability-reducers to self-healing stimulators 41 (2021).
[50] M. Roig-flores, F. Pirritano, P. Serna, L. Ferrara, Effect of crystalline admixtures on the self-healing capability of early-age concrete studied by means of permeability and crack closing tests, Constr. Build. Mater. 114 (2016) 447–457, https://doi.org/10.1016/j.conbuildmat.2016.03.196.
[51] P. Azarsa, R. Gupta, A. Biparva, Assessment of self-healing and durability parameters of concretes incorporating crystalline admixtures and Portland limestone cement, Cem. Concr. Compos. 99 (2019) 17–31, https://doi.org/10.1016/j.cemconcomp.2019.02.017.
[52] C. Xue, W. Li, Z. Luo, K. Wang, A. Castel, Effect of chloride ingress on self-healing recovery of smart cementitious composite incorporating crystalline admixture and MgO expansive agent, Cem. Concr. Res. 139 (2021), 106252, https://doi.org/10.1016/J.CEMCONRES.2020.106252.
[53] E. Cuenca, A. Tejedor, L. Ferrara, A methodology to assess crack-sealing effectiveness of crystalline admixtures under repeated cracking-healing cycles, Constr. Build. Mater. 179 (2018) 619–632, https://doi.org/10.1016/J.CONBUILDMAT.2018.05.261.
[54] K. Sisomphon, O. Copuroglu, E.A.B. Koenders, Effect of exposure conditions on self healing behavior of strain hardening cementitious composites incorporating various cementitious materials, Constr. Build. Mater. 42 (2013) 217–224, https://doi.org/10.1016/J.CONBUILDMAT.2013.01.012.
[55] E. Cuenca, A. Mezzena, L. Ferrara, Synergy between crystalline admixtures and nano-constituents in enhancing autogenous healing capacity of cementitious composites under cracking and healing cycles in aggressive waters, Constr. Build. Mater. 266 (2021), 121447, https://doi.org/10.1016/J.CONBUILDMAT.2020.121447.
[56] L. Ferrara, V. Krelani, F. Moretti, M. Roig, P. Serna, Effects of autogenous healing on the recovery of mechanical performance of high performance fibre reinforced cementitious composites (HPFRCCs): part 1, Cem. Concr. Compos. 83 (2017) 76–100, https://doi.org/10.1016/j.cemconcomp.2017.07.010.
[57] H. Doostkami, M. Roig-Flores, A. Negrini, E.J. Mezquida-Alcaraz, P. Serna, Evaluation of the self-healing capability of ultra-high-performance fiber-reinforced concrete with nano-particles and crystalline admixtures by means of permeability, in: Fibre Reinf. Concr. Improv. Innov. RILEM-Fib Int. Symp. FRC 2020 10, Springer, 2021, pp. 489–499.

[58] L. Ferrara, T. Van Mullem, M. Cruz, P. Antonaci, R. Paul, E. Cuenca, A. Jefferson, P. Ng, A. Peled, M. Roig-flores, M. Sanchez, C. Schroefl, P. Serna, D. Snoeck, J. Marc, N. De Belie, Experimental characterization of the self-healing capacity of cement based materials and its effects on the material performance : a state of the art report by COST action SARCOS WG2, Constr. Build. Mater. 167 (2018) 115–142, https://doi.org/10.1016/j.conbuildmat.2018.01.143.

[59] L. Ferrara, V. Krelani, F. Moretti, Autogenous healing on the recovery of mechanical performance of high performance fibre reinforced cementitious composites (HPFRCCs): part 2 e correlation between healing of mechanical performance and crack sealing, Cem. Concr. Compos. 73 (2016) 299–315, https://doi.org/10.1016/j.cemconcomp.2016.08.003.

[60] K.-S. L., C. D., J.-P. C., Self-healing of aged concrete containing crystalline admixture and expansive agent under repeated loading, J. Mater. Civ. Eng. 35 (2023) 4022396, https://doi.org/10.1061/(ASCE)MT.1943-5533.0004572.

[61] C. Zhang, R. Lu, Y. Li, X. Guan, Effect of crystalline admixtures on mechanical, self-healing and transport properties of engineered cementitious composite, Cem. Concr. Compos. 124 (2021), 104256, https://doi.org/10.1016/J.CEMCONCOMP.2021.104256.

[62] H. Zhu, D. Zhang, Y. Wang, T. Wang, V.C. Li, Development of self-stressing engineered cementitious composites (ECC), Cem. Concr. Compos. 118 (2021), 103936, https://doi.org/10.1016/j.cemconcomp.2021.103936.

[63] K. Yu, H. Zhu, M. Hou, V.C. Li, Self-healing of PE-fiber reinforced lightweight high-strength engineered cementitious composite, Cem. Concr. Compos. 123 (2021), 104209, https://doi.org/10.1016/j.cemconcomp.2021.104209.

[64] E. Yang, Designing Added Functions in Engineered Cementitious Composites, University of Michigan, 2008.

[65] L.L. Kan, H.S. Shi, Investigation of self-healing behavior of engineered cementitious composites (ECC) materials, Constr. Build. Mater. 29 (2012) 348–356, https://doi.org/10.1016/j.conbuildmat.2011.10.051.

[66] ASTM C215, Standard Test Method for Fundamental Transverse, Longitudinal, and Torsional Resonant Frequencies of Concrete Specimens, ASTM International, West Conshohocken, PA, 2019.

[67] K. Lauch, J. Charron, C. Desmettre, Comprehensive evaluation of self-healing of concrete with different admixtures under laboratory and long-term outdoor expositions, J. Build. Eng. 54 (2022), 104661, https://doi.org/10.1016/j.jobe.2022.104661.

[68] Y. Chen, F. Al-Neshawy, J. Punkki, Investigation on the effect of entrained air on pore structure in hardened concrete using MIP, Constr. Build. Mater. 292 (2021), 123441, https://doi.org/10.1016/j.conbuildmat.2021.123441.

[69] V.C. Li, C.K.Y. Leung, Steady-state and multiple cracking of short random fiber composites, J. Eng. Mech. 118 (1992) 2246–2264, https://doi.org/10.1061/(asce)0733-9399(1992)118:11(2246).

[70] Q.H. Lương, H.H. Nguyễn, J. Il Choi, H.K. Kim, B.Y. Lee, Effects of crumb rubber particles on mechanical properties and sustainability of ultra-high-ductile slag-based composites, Constr. Build. Mater. 272 (2021), 121959, https://doi.org/10.1016/j.conbuildmat.2020.121959.

[71] Z. Zhang, H. Ma, S. Qian, Investigation on properties of ECC incorporating crumb rubber of different sizes, J. Adv. Concr. Technol. 13 (2015) 241–251, https://doi.org/10.3151/jact.13.241.

[72] K.K. Aligizaki, Pore Structure of Cement-Based Materials: Testing, Interpretation and Requirements, 1st ed, Crc Press, 2005.

[73] H. Zhu, Q. Li, R. Ma, L. Yang, Y. Hu, J. Zhang, Water-repellent additive that increases concrete cracking resistance in dry curing environments, Constr. Build. Mater. 249 (2020), https://doi.org/10.1016/j.conbuildmat.2020.118704.

[74] M.H. Zhang, H. Li, Pore structure and chloride permeability of concrete containing nano-particles for pavement, Constr. Build. Mater. 25 (2011) 608–616, https://doi.org/10.1016/J.CONBUILDMAT.2010.07.032.

[75] D. Zhang, B. Jaworska, H. Zhu, K. Dahlquist, V.C. Li, Engineered cementitious composites (ECC) with limestone calcined clay cement (LC3), Cem. Concr. Compos. 114 (2020), 103766, https://doi.org/10.1016/j.cemconcomp.2020.103766.

[76] A. de Souza Oliveira, O. da Fonseca Martins Gomes, L. Ferrara, E. de Moraes Rego Fairbairn, R.D. Toledo Filho, An overview of a twofold effect of crystalline admixtures in cement-based materials: from permeability-reducers to self-healing stimulators, J. Build. Eng. 41 (2021), 102400, https://doi.org/10.1016/J.JOBE.2021.102400.